

BAM-DETR: Boundary-Aligned Moment Detection Transformer for Temporal Sentence Grounding in Videos

Pilhyeon Lee* Hyeran Byun

Department of Computer Science, Yonsei University

Abstract

Temporal sentence grounding aims to localize moments relevant to a language description. Recently, DETR-like approaches have shown notable progress by decoding the center and length of a target moment from learnable queries. However, they suffer from the issue of center misalignment raised by the inherent ambiguity of moment centers, leading to inaccurate predictions. To remedy this problem, we introduce a novel boundary-oriented moment formulation. In our paradigm, the model no longer needs to find the precise center but instead suffices to predict any anchor point within the interval, from which the onset and offset are directly estimated. Based on this idea, we design a Boundary-Aligned Moment Detection Transformer (BAM-DETR), equipped with a dual-pathway decoding process. Specifically, it refines the anchor and boundaries within parallel pathways using global and boundary-focused attention, respectively. This separate design allows the model to focus on desirable regions, enabling precise refinement of moment predictions. Further, we propose a quality-based ranking method, ensuring that proposals with high localization qualities are prioritized over incomplete ones. Extensive experiments verify the advantages of our methods, where our model records new state-of-the-art results on three benchmarks. Code is at <https://github.com/Pilhyeon/BAM-DETR>.

1. Introduction

Recent years have witnessed a notable surge in the popularity of short-form video content on social media platforms like YouTube Shorts, Instagram Reels, and TikTok. In the same vein, users prefer to selectively engage with short moments of interest rather than passively watch an entire long video. This trend highlights the importance of localizing desired moments. As a result, moment localization tasks have emerged as pivotal research topics in the field of video understanding, encompassing temporal action detection [20, 29, 75], highlight detection [22, 48, 58], and video

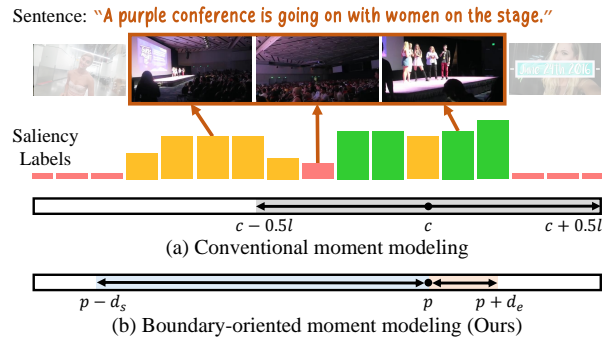


Figure 1. Comparison of moment modeling approaches under the scenario of an ambiguous center from QVHighlights [22]. (a) The conventional method formulates the moment with a tuple of (c, l) . (b) In contrast, we propose to model it with a triplet of (p, d_s, d_e) .

summarization [50, 71]. Within this context, we particularly tackle temporal sentence grounding [1], aiming to retrieve moments corresponding to free-form language descriptions.

To address temporal sentence grounding, numerous efforts have been undertaken in the last decade [9, 11, 32, 49, 63, 73]. Especially, taking inspiration from DETR [3], query-based approaches have become a promising research direction owing to the architectural simplicity [17, 22, 26, 37, 41]. By decoding temporal spans from a small set of learnable queries, they achieve promising grounding performance while maintaining high inference speed.

Existing query-based models typically predict a moment using its center and width, *i.e.*, (c, l) , under the assumption that the boundaries are equidistant from the center. However, such a formulation can be problematic as the center of a moment might be ambiguous. An illustrative example is presented in Fig. 1 (top), where the frame at the center of the ground-truth moment primarily shows the audience, which is less relevant to the given sentence. This ambiguity can challenge the model’s ability to precisely locate the centers, resulting in low-quality predictions (Fig. 1a). To probe the impact of center misalignment on performance, we conducted a diagnostic experiment in Table 1. The results reveal that existing methods struggle with detecting accurate center points and suffer from significant performance drops when the predicted centers deviate from the ground truths.

*Correspondence to: Pilhyeon Lee <lph1114@yonsei.ac.kr>

Method	[0, 0.1)	[0.1, 0.2)	[0.2, 0.3)	[0.3, 0.4)	[0.4, 0.5)	All
M-DETR [22]	83.20 (46 %)	65.00 (24 %)	54.82 (14 %)	43.77 (9 %)	34.98 (7 %)	67.84 (100 %)
QD-DETR [41]	87.79 (56 %)	67.95 (18 %)	55.40 (11 %)	44.93 (9 %)	36.45 (5 %)	74.09 (100 %)
BAM-DETR [†] (Ours)	77.62 (24 %)	78.20 (21 %)	77.52 (21 %)	78.96 (22 %)	71.08 (12 %)	77.21 (100 %)

[†]anchor points are utilized for grouping.

Table 1. Impact of misaligned centers on QVHighlights [22]. The top-1 predictions are grouped based on their center errors normalized by ground-truth lengths. For each group, we present the mean IoU (%) and the proportion (in parentheses). Only the predictions whose centers fall within the ground truths are considered here¹.

To address the challenge, we present a novel boundary-oriented formulation for moments, as illustrated in Fig. 1b, where each moment is represented by a triplet consisting of an anchor point and its distances to the boundaries, *i.e.*, (p, d_s, d_e) . This formulation liberates the model from the stringent requirement of predicting the center. Instead, it is sufficient for the model to predict any salient anchor within the target moment, and the distances from the anchor to the onset and offset are predicted subsequently. By directly locating the boundaries based on the anchor point, the model can achieve improved boundary alignment, even when the anchor point does not coincide with the actual center.

Building upon the proposed moment modeling, we introduce a new framework equipped with a dedicated decoder, dubbed Boundary-Aligned Moment Detection Transformer (BAM-DETR). The design of its decoding layers originates from the intuition that the refining processes for an anchor and boundaries should be distinct from each other. That is to say, a model needs to scan over the whole video to find a potential anchor point that enables estimating the rough location of the target moment. On the other hand, it is required to focus on fine-grained details in the vicinity to refine the boundaries to be aligned with those of the target moments. From this motivation, in contrast to existing methods, our model adopts a dual-pathway decoding pipeline to predict an anchor point and boundaries in a parallel way. To be specific, we leverage two different types of queries respectively for anchor and boundary refinement. The former aggregates global information with standard attention, while the latter concentrates on the sparse local neighborhood of the boundaries using the proposed boundary-focused attention. These distinct designs of two pathways allow for effective moment localization with minimal computational overhead increase.

In addition, we identify the problem of the conventional scoring method, where binary classification (or matching) scores are used for proposal ranking. This leads to suboptimal results for the grounding task since a fractional moment may have high matching scores with the given sen-

tence. To handle this issue, we propose to rank proposals based on their localization qualities. Accordingly, we modify the typical matching function and training objectives to be localization-oriented by discarding the role of classification scores. In this way, our model can prioritize the moment proposals exhibiting high overlap with ground truths at inference, leading to improved grounding performance.

The advantage of our BAM-DETR over existing methods is shown in Table 1. It is observed that the anchor points predicted by our model are evenly distributed within the ground-truth intervals. Importantly, our model consistently produces precise moments with high IoUs (> 0.7) across different groups, indicating that it does not depend on center prediction. On average, our model shows superior grounding performances with the help of our moment formulation and quality-based scoring. In a later section, we validate the effectiveness of the proposed methods through extensive experiments. Notably, our model outperforms previous state-of-the-art methods by large margins on three public benchmarks, especially under strict evaluation metrics.

2. Related Works

2.1. Temporal Sentence Grounding in Videos

Temporal sentence grounding requires seeking temporal spans semantically relevant to the given sentence in a video. Proposal-based approaches adopt the two-stage pipeline, *i.e.*, proposal generation and ranking. They generate moment proposals by relying on sliding windows [11, 13, 34, 72] or utilizing pre-defined anchors [4, 59, 63, 67, 74]. Several works process all possible candidates at once with 2D maps [25, 31, 56, 57, 73]. On the other hand, proposal-free methods are developed for efficient grounding by directly predicting the moments [42, 64] or estimating the probabilities of each frame being starting and ending positions [15, 69]. Several approaches perform dense regression by predicting the boundaries from individual frames [5, 39, 66]. Recently, query-based models streamline the complicated sentence grounding pipeline by removing handcrafted techniques [2, 17, 26, 37, 60]. There are also attempts to unify temporal sentence grounding with other video understanding tasks into a single framework [28, 61].

Our method belongs to the query-based group [22, 41], inheriting the benefit of architectural simplicity. In contrast to others, we employ a new boundary-oriented formulation of moments so as to relieve the heavy reliance on center predictions, leading to better boundary alignment. Meanwhile, our method also relates to the dense regression methods [5, 28, 39, 66] that predict distances to the boundaries considering each frame an anchor. Compared to them, our model leverages dynamic anchor points that are gradually adjusted for better prediction through decoding, enabling precise localization with a small number of predictions.

¹In case of interest, the mean IoUs of the predictions with their centers falling outside the ground truths are 11.76, 12.46, and 22.51, respectively.

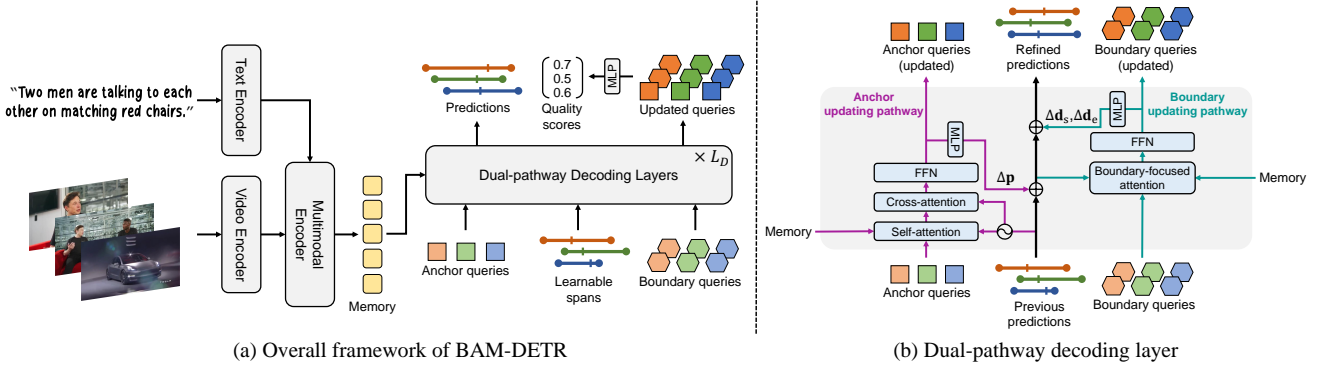


Figure 2. (a) Overview of the proposed BAM-DETR. (b) Details of the proposed dual-pathway decoding layer. It consists of two parallel pathways respectively for anchor and boundary updates, which refine the previous moment predictions in a sequential manner.

2.2. Detection Transformers

Query-based temporal sentence grounding models by design are closely related to the family of detection transformer (DETR) [3]. Since the advent of DETR, a number of variants have been introduced to improve it from various perspectives [30, 33, 36, 53]. Some works focus on reducing the excessive computational costs of vanilla transformers to leverage multi-scale features [7, 24, 47, 76, 78]. Other methods attempt to speed up the model convergence by manipulating the attention operations [12, 35, 62, 68] or incorporating the denoising process during the training [23, 70].

The most relevant ones to ours are those which propose explicit anchor modeling for object queries with points [40, 55] or boxes [35, 78]. In comparison to an object, a moment in temporal sentence grounding has its own challenges such as center ambiguity and indistinct boundaries. To accommodate the discrepancies, we propose a novel boundary-oriented modeling of moments to replace the conventional 1D box-based modeling. The advantages of our approach are clearly verified in the experiments.

3. Method

Given an untrimmed video and a sentence, the goal of temporal sentence grounding is to localize relevant moments $\{\varphi_n = (t_{s_n}, t_{e_n})\}_{n=1}^N$, where N denotes the number of ground truths in the video and φ_n indicates the temporal interval of the n -th moment. Note that a video may have multiple moments that match the sentence, *i.e.*, $N \geq 1$. During the test time, the model is expected to produce a total of M predictions, $\{(\hat{\varphi}_m, q_m)\}_{m=1}^M$, where $\hat{\varphi}_m = (\hat{t}_{s_m}, \hat{t}_{e_m})$ is the m -th prediction, while q_m is its score for ranking.

Motivation. We tackle two main problems in the current prediction process. On one hand, existing query-based approaches adopt the symmetric design of (c, l) to predict a moment, *i.e.*, $\hat{\varphi} = (c - 0.5l, c + 0.5l)$. As we discuss in Sec. 1, this strategy suffers from the issue of over-reliance on the center prediction, leading to unstable performances.

To address this, we propose a boundary-oriented modeling with a triplet of (p, d_s, d_e) , where a moment is represented by $\hat{\varphi} = (p - d_s, p + d_e)$. This asymmetric design enables direct alignment of boundaries without relying on precise prediction of the center. On the other hand, previous models utilize the classification score as q_m . This scoring is prone to sub-optimal solutions since only a fraction of the moment may well match the sentence, leading incomplete predictions to be highly ranked. To handle this, we propose quality-based scoring to sort the proposals based on their localization qualities rather than the degree of matching.

3.1. Overview

As shown in Fig. 2a, our BAM-DETR follows the encoder-decoder pipeline. Briefly, it first extracts multimodal video features using the encoders. Taking them as memory, the boundary-aligning decoder predicts a set of temporal spans and their quality scores by progressively refining learnable initial spans using anchor and boundary queries.

3.2. Feature Extraction

Following the convention [42, 69, 73], we employ pre-trained encoders for token-level unimodal feature extraction. It is worth noting that all unimodal encoders are kept frozen during training to avoid memory exploding. In this stage, we obtain D_v -dim video features $E_v \in \mathbb{R}^{N_v \times D_v}$ and D_t -dim text features $E_t \in \mathbb{R}^{N_t \times D_t}$, where N_v and N_t are the numbers of clips and words, respectively.

3.3. Multimodal Encoder

We feed the unimodal features of the video and text to the multimodal encoder, so as to fuse them into text-aware video representations for temporal sentence grounding. While various multimodal encoders are explored [22, 28, 37], we adopt the text-to-video encoder design [41] consisting of cross- and self-attention blocks [54]. Before getting into the encoder, unimodal features are projected into a shared space to facilitate cross-modal interaction, *i.e.*, $\mathcal{V} = f_v(E_v) \in \mathbb{R}^{N_v \times D}$, $\mathcal{T} = f_t(E_t) \in \mathbb{R}^{N_t \times D}$, where D

is the embedding dimension. Afterward, multi-head cross-attention blocks are used to inject textual information into the clip-level video representations. In specific, we project \mathcal{V} to $\mathbf{Q}_{\mathcal{V}}$ (query) while \mathcal{T} to $\mathbf{K}_{\mathcal{T}}$ (key) and $\mathbf{V}_{\mathcal{T}}$ (value). Then a single-head attention block can be formulated as:

$$\begin{aligned}\mathcal{V}' &= \text{softmax}\left(\frac{\mathbf{Q}_{\mathcal{V}}\mathbf{K}_{\mathcal{T}}^{\top}}{\sqrt{D}}\right)\mathbf{V}_{\mathcal{T}} + \mathcal{V}, \\ \mathcal{V}'' &= \text{FFN}(\mathcal{V}') + \mathcal{V}',\end{aligned}\quad (1)$$

where $\text{FFN}(\cdot)$ is a feed-forward network. We denote the resulting multimodal representations obtained after L_E multi-head cross-attention blocks by $\hat{\mathcal{V}} \in \mathbb{R}^{N_v \times D}$. Although we here present the single-head attention block, it can readily generalize to a multi-headed version [54].

Subsequently, self-attention blocks are leveraged to enhance the representations by allowing the inter-clip interaction. Here we project $\hat{\mathcal{V}}$ to $\mathbf{Q}_{\hat{\mathcal{V}}}$, $\mathbf{K}_{\hat{\mathcal{V}}}$, and $\mathbf{V}_{\hat{\mathcal{V}}}$. We note that the query and the key are supplemented with fixed sinusoidal positional encoding [3, 54] for temporal awareness. Then the self-attention block is defined in a similar way to Eq. (1) but with different inputs. The enhanced clip-level representations after L_E self-attention blocks are denoted by $\hat{\mathcal{V}} \in \mathbb{R}^{N_v \times D}$, which serves as *memory* for the decoder.

It is widely known that providing the multimodal features with saliency guidance helps the model to better understand the semantic relationship between the video and text [22, 28]. As in the previous works [17, 26], we impose saliency score constraints on the memory features. Specifically, we leverage a saliency predictor $S(\cdot)$ and train the model with the following margin-based training objective.

$$\mathcal{L}_{\text{margin}} = \max(0, \alpha + S(\hat{v}^{\text{low}}) - S(\hat{v}^{\text{high}})), \quad (2)$$

where α is a margin and $(\hat{v}^{\text{low}}, \hat{v}^{\text{high}})$ is the sampled feature pair satisfying that the saliency label of \hat{v}^{low} is lower than that of \hat{v}^{high} . In case of the absence of saliency labels, we collect clips within and outside the ground-truth moment intervals. In addition, we employ the rank-aware contrastive loss $\mathcal{L}_{\text{cont}}$ and the negative relation loss \mathcal{L}_{neg} , following Moon *et al.* [41]. Due to space limits, we refer the readers to Appendix for the loss formulations. In summary, the overall saliency loss is defined as $\mathcal{L}_{\text{sal}} = \mathcal{L}_{\text{margin}} + \mathcal{L}_{\text{cont}} + \mathcal{L}_{\text{neg}}$.

3.4. Dual-pathway Decoder

With the multimodal representations $\hat{\mathcal{V}}$ as memory features, we aim to localize temporal spans corresponding to the sentence. We adopt the new boundary-oriented formulation for moment prediction, where each prediction is represented by a triplet of (p, d_s, d_e) , where p is the anchor point, while d_s and d_e are the distances from the anchor to the starting and ending points, respectively. To make full use of the modified formulation, we design a dual-pathway decoding layer with two parallel pathways as described in Fig. 2b. The

inputs of the l -th layer are anchor queries $\mathbf{C}_p^l \in \mathbb{R}^{M \times D}$, boundary queries $\mathbf{C}_s^l, \mathbf{C}_e^l \in \mathbb{R}^{M \times D}$, and previous moment predictions $\mathbf{A}^l = [\mathbf{p}^l; \mathbf{d}_s^l; \mathbf{d}_e^l] \in \mathbb{R}^{M \times 3}$, where M is the number of queries (predictions). Note that the initial queries and spans, *i.e.*, $\{\mathbf{C}_p^0, \mathbf{C}_s^0, \mathbf{C}_e^0, \mathbf{A}^0\}$, are learnable parameters. We elaborate on the two pathways in the following.

Anchor updating pathway. Given the predictions and the anchor queries from the preceding layer, the goal of this pathway is to adjust the anchor position so that the boundaries can be accurately predicted based on it. Intuitively, in order to obtain a valuable anchor point without redundancy, an anchor query should communicate with other queries as well as the memory features. To this goal, the anchor updating pathway consists of a self-attention layer, a cross-attention layer, and a feed-forward network. In the self-attention layer, the anchor queries \mathbf{C}_p^l are first projected into $\mathbf{Q}_{\mathbf{C}_p^l}$, $\mathbf{K}_{\mathbf{C}_p^l}$, and $\mathbf{V}_{\mathbf{C}_p^l}$. Since an anchor query itself lacks positional information, we build positional encoding. Following the previous works [17, 41], we extend the current spans \mathbf{A}^l to the positional information of the queries, *i.e.*, $\mathbf{P}_{\mathbf{A}^l} = \text{MLP}(\text{PE}(\mathbf{A}^l)) \in \mathbb{R}^{M \times D}$, where $\text{PE}(\cdot)$ denotes the point-wise mapping from a position to the corresponding sinusoidal encoding while $\text{MLP}(\cdot)$ is multi-layer perceptron. Then, the self-attention for the anchor queries is defined as:

$$\tilde{\mathbf{C}}_p^l = \text{softmax}\left(\frac{(\mathbf{Q}_{\mathbf{C}_p^l} + \mathbf{P}_{\mathbf{A}^l})(\mathbf{K}_{\mathbf{C}_p^l} + \mathbf{P}_{\mathbf{A}^l})^{\top}}{\sqrt{D}}\right)\mathbf{V}_{\mathbf{C}_p^l} + \mathbf{C}_p^l. \quad (3)$$

After inter-query interaction, we employ a global cross-attention layer to aggregate multi-modal features from the memory. The anchor query $\tilde{\mathbf{C}}_p^l$ is projected into $\mathbf{Q}_{\tilde{\mathbf{C}}_p^l}$ while the memory $\hat{\mathcal{V}}$ is projected into $\mathbf{K}_{\hat{\mathcal{V}}}$ and $\mathbf{V}_{\hat{\mathcal{V}}}$. To make the query location-aware, we leverage the sinusoidal encoding of current anchor positions, *i.e.*, $\mathbf{P}_{\mathbf{p}^l} = \text{PE}(\mathbf{p}^l) \in \mathbb{R}^{M \times D}$. Similarly, the memory leverages the positional encoding, *i.e.*, $\mathbf{P}_{\hat{\mathcal{V}}} = \text{PE}(\hat{\mathcal{V}}) \in \mathbb{R}^{N_v \times D}$. We use concatenation instead of summation to separate the roles of features and positional encoding [35, 40]. Then the global cross-attention between anchor queries and the memory can be expressed as follows.

$$\hat{\mathbf{C}}_p^l = \text{softmax}\left(\frac{(\mathbf{Q}_{\tilde{\mathbf{C}}_p^l} \parallel \mathbf{P}_{\mathbf{p}^l})(\mathbf{K}_{\hat{\mathcal{V}}} \parallel \mathbf{P}_{\hat{\mathcal{V}}})^{\top}}{\sqrt{2D}}\right)\mathbf{V}_{\hat{\mathcal{V}}} + \tilde{\mathbf{C}}_p^l. \quad (4)$$

Then the anchor queries are updated with a feed-forward network, *i.e.*, $\mathbf{C}_p^{(l+1)} = \text{FFN}(\hat{\mathbf{C}}_p^l) + \hat{\mathbf{C}}_p^l$. Lastly, we adjust the anchor positions using sigmoid-based refinement [78]: $\hat{\mathbf{A}}^l = [\mathbf{p}^{(l+1)}; \mathbf{d}_s^l; \mathbf{d}_e^l]$ where $\mathbf{p}^{(l+1)} = \sigma(\sigma^{-1}(\mathbf{p}^l) + \Delta\mathbf{p}^l)$ with $\Delta\mathbf{p}^l = \text{MLP}(\mathbf{C}_p^{(l+1)}) \in \mathbb{R}^M$ and sigmoid function σ .

Boundary updating pathway. After the anchor update, we need to refine the boundaries based on the anchor. It

is widely perceived that a model needs to focus on fine-grained features in the neighborhood rather than far ones to adjust temporal boundaries [27, 29, 51]. Inspired by this, we devise a boundary-focused attention layer (Fig. 3). For brevity, we explain the process of starting point update.

The plain memory $\hat{\mathcal{V}}$ lacks the inductive bias due to the property of attentional layers [8]. Thus we first build locality-enhanced memory features for effective boundary refinement. To this goal, we obtain boundary-sensitive features with several 1D convolutional layers, *i.e.*, $\hat{\mathcal{V}}'_s = f_s(\hat{\mathcal{V}})$. Then we encourage them to highly activate around the starting position of target moments. In detail, on the clip-wise activation scores obtained by channel-mean, *i.e.*, $\hat{g}^s = \text{mean}(\sigma(\hat{\mathcal{V}}_s)) \in \mathbb{R}^{N_v}$, we impose regularization as:

$$\mathcal{L}_{\text{regul}}^s = -\frac{1}{N_v} \sum_{i=1}^{N_v} (g_i^s \log(\hat{g}_i^s) + (1 - g_i^s) \log(1 - \hat{g}_i^s)), \quad (5)$$

where g_i^s is the binary label obtained as $g_i^s = \mathbb{1}[i \in \mathcal{B}^s]$, where \mathcal{B}^s is the neighbor clip set around starting points with a radius of r^s . We merge boundary-sensitive features with the plain ones to form locality-enhanced memory, *i.e.*, $\hat{\mathcal{V}}'_s = [\hat{\mathcal{V}} \parallel \hat{\mathcal{V}}'_s] \in \mathbb{R}^{N_v \times 2D}$. We can obtain $\mathcal{L}_{\text{regul}}^e$ and $\hat{\mathcal{V}}'_e$ in the same way. The total regularization term is $\mathcal{L}_{\text{regul}} = \mathcal{L}_{\text{regul}}^s + \mathcal{L}_{\text{regul}}^e$.

Given the locality-enhanced memory, the queries need to capture fine-grained details around the boundaries for refinement. To aggregate useful features near the boundaries, we employ deformable attention [77, 78]. Regarding the starting boundary ($\mathbf{p}^{(l+1)} - \mathbf{d}_s^l$) as the origin, we predict offsets and weights to select K neighbors, *i.e.*, $\mathbf{o}^s = \phi_o(\mathbf{C}_s^l) \in \mathbb{R}^{M \times K}$, $\mathbf{w}^s = \text{softmax}(\phi_w(\mathbf{C}_s^l)) \in \mathbb{R}^{M \times K}$, where ϕ_* are fully-connected layers. Features from the sampled neighbors are then aggregated into the starting queries as:

$$\hat{\mathbf{C}}_s^l = \sum_{k=1}^K [\mathbf{w}_k^s \cdot \hat{\mathcal{V}}'_s[\mathbf{p}^{(l+1)} - \mathbf{d}_s^l + \mathbf{o}_k^s]] + \mathbf{C}_s^l, \quad (6)$$

where we denote the sampling process from memory by $\hat{\mathcal{V}}'_s[\cdot]$. Lastly, we adopt a feed-forward network to obtain the updated starting queries, *i.e.*, $\mathbf{C}_s^{(l+1)} = \text{FFN}(\hat{\mathbf{C}}_s^l)$. We also obtain $\mathbf{C}_e^{(l+1)}$ in the same way. Using boundary queries, we refine the boundaries to be better aligned with those of ground truths, *i.e.*, $\mathbf{A}^{(l+1)} = [\mathbf{p}^{(l+1)}; \mathbf{d}_s^{(l+1)}; \mathbf{d}_e^{(l+1)}]$ with sigmoid-based refinement as similar in the anchor update. Note that we utilize deformable attention for the purpose of local feature aggregation, which differs from the work [78] that uses it for efficient multi-scale global operation. We provide comparison experiments of their roles in Appendix.

Moment prediction. We repeatedly update the predictions through a total of L_D dual-pathway decoding layers. We denote the final predictions by $\mathbf{A} = [\mathbf{p}; \mathbf{d}_s; \mathbf{d}_e]$, the anchor queries by \mathbf{C}_p , and the boundary queries by \mathbf{C}_s and \mathbf{C}_e . Then we cast the final predictions in the form of starting and ending timestamps, *i.e.*, $\hat{\varphi} = [\mathbf{p} - \mathbf{d}_s; \mathbf{p} + \mathbf{d}_e] \in \mathbb{R}^{M \times 2}$, which will serve as the final moment prediction results.

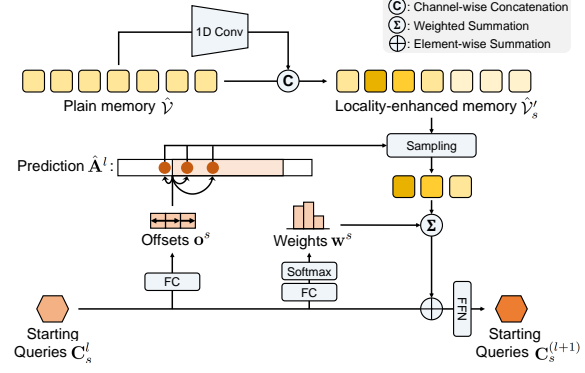


Figure 3. Boundary-focused attention layer for starting queries.

3.5. Quality-based Scoring

After producing the moment predictions, we opt to rank them for evaluation. In the convention, query-based models utilize classification scores as the measure, which exhibits how well the proposals semantically match the sentence. However, it does not necessarily represent the localization qualities of proposals. Hence we propose to estimate the localization quality of each moment prediction. Owing to the complementarity of anchor and boundary queries, we leverage all of them to predict the quality scores of the current predictions. Formally, the quality score can be derived as $\mathbf{q} = \sigma(\text{MLP}([\mathbf{C}_p \parallel \mathbf{C}_s \parallel \mathbf{C}_e])) \in \mathbb{R}^M$, where σ is sigmoid activation. The quality loss is defined as follows.

$$\mathcal{L}_{\text{qual}} = \sum_{m=1}^M \left| q_m - \max_{\varphi_n} \left(\frac{|\hat{\varphi}_m \cap \varphi_n|}{|\hat{\varphi}_m \cup \varphi_n|} \right) \right|, \quad (7)$$

where the objective of the quality head is to predict the maximum IoUs of the proposals with ground-truth moments.

3.6. Matching

Following the standard [3, 22], we perform Hungarian matching [19] between predictions and ground truths. The optimal matching results ψ^* can be derived as follows.

$$\psi^* = \arg \min_{\psi \in \mathcal{G}_N} \sum_{n=1}^N \mathcal{C}(\varphi_n, \hat{\varphi}_{\psi(n)}),$$

$\mathcal{C}(\varphi_n, \hat{\varphi}_{\psi(n)}) = \lambda_{l_1} \mathcal{L}_{l_1}(\varphi_n, \hat{\varphi}_{\psi(n)}) + \lambda_{\text{iou}} \mathcal{L}_{\text{iou}}(\varphi_n, \hat{\varphi}_{\psi(n)})$, where \mathcal{G}_N denotes the combination pool and $\psi(n)$ is the index of the prediction matched by the n -th ground truth. \mathcal{L}_{l_1} and \mathcal{L}_{iou} respectively represent the L_1 distance and the generalized IoU [46] between the moments, while λ_{l_1} and λ_{iou} are their weights. Note that in contrast to other works, the classification term is not involved in the matching process.

Once the matching is completed, we minimize the matching cost between each pair of the matching results ψ^* . The moment localization loss can be formulated as follows.

$$\mathcal{L}_{\text{loc}} = \sum_{n=1}^N \mathcal{C}(\varphi_n, \hat{\varphi}_{\psi^*(n)}). \quad (8)$$

Overall training objectives. Our model is trained in an end-to-end fashion and the overall objective is defined as:

$$\mathcal{L}_{\text{total}} = \mathcal{L}_{\text{loc}} + \lambda_{\text{qual}}\mathcal{L}_{\text{qual}} + \lambda_{\text{sal}}\mathcal{L}_{\text{sal}} + \lambda_{\text{regul}}\mathcal{L}_{\text{regul}}, \quad (9)$$

where λ_* are the balancing parameters.

4. Experiments

4.1. Experimental Settings

Datasets. QVHighlights [22] is a recently built dataset, containing a total of 10,148 videos and 10,310 sentences from vlog and news domains. In addition to moments, it provides segment-level saliency score annotations within each moment. Importantly, it allows a single sentence corresponding to multiple disjoint moments (1.8 on average). Due to this practical setup, we utilize QVHighlights as the main benchmark for experiments. Charades-STA [11] includes 16,128 sentence-moment pairs with 9,848 indoor videos. The average duration of videos and moments is 30.6 and 8.1 seconds, respectively. TACoS [45] contains 127 cooking videos encompassing a total of 18,818 sentence-moment pairs. This dataset is known to be challenging since the moments occupy only a small portion (6.1 sec on average) within considerably long videos (4.8 min on average).

Evaluation metrics. Following the standard protocol, we measure the Recall@1 (R1) under the IoU thresholds of 0.3, 0.5, and 0.7 by default. Since QVHighlights contains multiple ground-truth moments per sentence, we report the mean average precision (mAP) with IoU thresholds of 0.5 and 0.75 as well as the average mAP over a set of IoU thresholds [0.5:0.05:0.95]. Meanwhile, we compute the mean IoU of top-1 predictions on Charades-STA and TACoS. Note that the performances at high IoU thresholds (*e.g.*, 0.7) exhibit how well the predictions align with the ground truths.

4.2. Implementation Details

For a fair comparison, we adopt the same feature extraction strategy with the competitors [22, 26, 41]. Specifically, we adopt the CLIP [44] text features for text and the concatenation of Slowfast [10] (ResNet-50) and CLIP [44] (ViT-B/32) features for videos unless otherwise specified. The video features are extracted every 1 second for Charades-STA and 2 seconds for QVHighlights and TACoS. To compare with audio-augmented models [37], we optionally employ audio features extracted by PANNs [18] pre-trained on AudioSet [14]. Due to the long video duration, we uniformly sample 200 feature vectors from each video for TACoS.

We set the embedding dimension D to 256, the number of attention heads to 8, the number of queries M to 10, the number of boundary points K to 3, and the margin α to 0.2. We determine the numbers of encoding and decoding layers as same with the prior work [41], *i.e.*, $L_E = L_D = 2$. The balancing parameters are set as: $\lambda_{l1} = 10$, $\lambda_{\text{iou}} = \lambda_{\text{sal}} = \lambda_{\text{regul}} = 1$, $\lambda_{\text{qual}} = 2$. As in previous works [26, 41], we

Method	R1		mAP		
	@0.5	@0.7	@0.5	@0.75	Avg.
<i>w/o pre-training</i>					
MCN [1]	11.41	2.72	24.94	8.22	10.67
CAL [9]	25.49	11.54	23.40	7.65	9.89
CLIP [44]	16.88	5.19	18.11	7.00	7.67
XML [21]	46.69	33.46	47.89	34.67	34.90
Moment-DETR [22]	52.89	33.02	54.82	29.40	30.73
UMT [†] [37]	56.23	41.18	53.83	37.01	36.12
MH-DETR [60]	60.05	42.48	60.75	38.13	38.38
QD-DETR [41]	62.40	44.98	62.52	39.88	39.86
QD-DETR [†] [41]	63.06	45.10	63.04	40.10	40.19
UniVTG [28]	58.86	40.86	57.60	35.59	35.47
EaTR [‡] [17]	57.98	42.41	59.95	39.29	39.00
MomentDiff [26]	57.42	39.66	54.02	35.73	35.95
BAM-DETR	62.71	48.64	64.57	46.33	45.36
BAM-DETR [†]	64.07	48.12	65.61	47.51	46.91
<i>w/ pre-training on 4.2M data labeled by CLIP</i>					
UniVTG [28]	65.43	50.06	64.06	45.02	43.63
<i>w/ pre-training on 236K ASR captions</i>					
Moment-DETR [22]	59.78	40.33	60.51	35.36	36.14
UMT [†] [37]	60.83	43.26	57.33	39.12	38.08
QD-DETR [41]	63.18	45.19	63.37	40.35	39.96
BAM-DETR	63.88	47.92	66.33	48.22	46.67

[†]additional use of audio modality [‡]reproduced by official checkpoint

Table 2. Results on the QVHighlights test split.

increase λ_{sal} to 4 when saliency labels are unavailable, *i.e.*, for Charades-STA and TACoS. Our model is trained from scratch for 200 epochs on QVHighlights and 100 epochs on the other datasets using the AdamW optimizer [38] with a learning rate of 1e-4 and a batch size of 32.

4.3. Comparison with State-of-the-arts

Results on QVHighlights. We compare our model with existing state-of-the-arts including recent query-based approaches [17, 22, 26, 37, 41, 60] on the test split². As shown in Table 2, our BAM-DETR consistently outperforms the comparative models under various settings. In detail, without pre-training, our model surpasses the previous state-of-the-art model [41] by large margins, *e.g.*, 3.66% in R1@0.7 and 6.45% in mAP@0.75. These improvements under strict IoU thresholds verify the superior localization ability of our method. When leveraging the audio features, the performance further boosts especially in R1@0.5 and mAPs, enlarging the gap between the competitors including those with audio features [37, 41]. To compare with the methods with pretraining, we pretrain our model on middle-scale ASR caption data [22]. Again, our BAM-DETR achieves state-of-the-art results, while showing the least gap with the method [28] that leverages large-scale data for pre-training. Notably, our model even outperforms it in terms of mAPs with much fewer (about 18 \times) pre-training data, manifesting the effectiveness of the proposed methods.

²Codalab QVHighlights Evaluation Server

Method	R1@0.3	R1@0.5	R1@0.7	mIoU
2D-TAN [73]	58.76	46.02	27.40	41.25
VSLNet [69]	60.30	42.69	24.14	41.58
Moment-DETR [22]	65.83	52.07	30.59	45.54
QD-DETR [41]	-	57.31	32.55	-
UniVTG [28]	70.81	58.01	35.65	50.10
MomentDiff [26]	-	55.57	32.42	-
BAM-DETR	72.93	59.95	39.38	52.33

Table 3. Results on the Charades-STA test split.

Method	R1@0.3	R1@0.5	R1@0.7	mIoU
2D-TAN [73]	40.01	27.99	12.92	27.22
VSLNet [69]	35.54	23.54	13.15	24.99
Moment-DETR [22]	37.97	24.67	11.97	25.49
QD-DETR [‡] [41]	52.39	36.77	21.07	35.76
UniVTG [28]	51.44	34.97	17.35	33.60
MomentDiff [‡] [26]	46.64	28.92	12.37	30.36
BAM-DETR	56.69	41.54	26.77	39.31

[‡]reproduced by official codebase

Table 4. Results on the TACoS test split.

Results on Charades-STA. Experimental results on the test split are shown in Table 3. Not only does our BAM-DETR outperform the query-based competitors [22, 26, 41], but it achieves a new state-of-the-art by surpassing the best performing anchor-free model [28] for all metrics. Notably, a large performance gap of 3.73% is observed in R1@0.7, which confirms the strong localization ability of our model.

Results on TACoS. We present the comparison results on the test set in Table 4. It can be observed that our BAM-DETR achieves a new state-of-the-art with pronounced performances under the strict IoU thresholds, which is consistent with the above results on other datasets. On this challenging benchmark, our model surpasses the previous best model [41] by 5.7% (relatively 27%) in R1@0.7. These results clearly exhibit the superiority of the proposed model.

4.4. Robustness Evaluation

Query-based models potentially have a temporal bias [16, 65] against the locations and lengths of moments. To measure robustness, we evaluate our model on the anti-biased Charades-STA [26] with distribution shifts of the moment location and length between training and test sets. Table 5 summarizes the results, where our model outperforms all competitors under both anti-biased settings. Especially, it shows significant performance gaps under the moment length bias. This can be expected since our model directly localizes boundaries instead of predicting lengths, which lessens the effect of bias. This robustness test corroborates the advantage of our boundary-oriented moment modeling.

4.5. Analysis

We conduct analytic experiments on the QVHighlights validation split. More experiments are included in Appendix.

Method	R1@0.3	R1@0.5	R1@0.7	mAP _{avg}
<i>w.r.t. moment location</i>				
2D-TAN [73]	27.81	20.44	10.84	17.23
MMN [56]	33.58	27.20	14.12	19.18
Moment-DETR [22]	29.94	22.16	11.56	18.66
QD-DETR [‡] [41]	56.17	46.82	28.13	30.70
MomentDiff [26]	48.39	33.59	15.71	21.37
BAM-DETR	59.83	50.00	32.08	31.68
<i>w.r.t. moment length</i>				
2D-TAN [73]	39.68	28.68	17.72	22.79
MMN [56]	43.58	34.31	19.94	26.85
Moment-DETR[22]	42.73	34.39	16.12	24.02
QD-DETR [‡] [41]	67.39	54.44	32.87	36.99
MomentDiff [26]	51.25	38.32	23.38	28.19
BAM-DETR	68.40	55.46	40.74	43.21

[‡]reproduced by official codebase

Table 5. Results on the anti-biased Charades-STA test split against the moment length and location. To enable a fair comparison, the VGG [52] and Glove [43] features are employed for all models.

Method	R1		mAP		
	@0.5	@0.7	@0.5	@0.75	Avg.
Baseline	62.39	47.87	62.64	41.54	41.75
+ boundary-oriented modeling	63.42	49.23	62.86	43.24	42.42
+ dual-pathway decoder	63.61	50.26	63.01	44.98	44.16
+ quality-based scoring	65.10	51.61	65.41	48.56	47.61

Table 6. Ablation study of components on QVHighlights.

Effect of each component. We analyze the effect of each component in Table 6. The direct adoption of our moment modeling solely improves the performance, particularly at strict thresholds, showcasing its advantage in boundary alignment. Employing the dual-pathway decoder leads to further gains, which suggests the essential role of separate pathways. Lastly, the quality-based scoring considerably elevates the scores, especially in terms of mAPs.

Number of predictions. We experiment with varying numbers of predictions in Table 7a, where the model achieves robust results when M is sufficiently large. By default, we set M to 10 as same with the previous works [22, 41].

Locality-enhanced features. We analyze the effect of the choice of input features for boundary-focused attention in Table 7b. The results indicate that boundary-sensitive features are more helpful than plain ones in precise localization. In addition, owing to their complementarity, the merged features enable achieving the best performance.

Number of sampled boundary points. We analyze the effect of the number of sampled boundary points K in Table 7c. For comparisons, we report the case where the fixed boundary features are sampled without using offsets (1st row). As shown in the table, the dynamic selection of neighborhoods rather than fixed boundaries is important for accurate moment localization. The performance improves when sampling multiple points, while it saturates at $K = 3$.

M	R1		mAP		
	@0.5	@0.7	@0.5	@0.75	Avg.
5	62.19	49.03	62.26	46.50	45.18
10	65.10	51.61	65.41	48.56	47.61
15	65.48	50.32	65.34	49.77	48.23
20	65.23	51.61	64.56	49.40	48.01

(a) Number of predictions

Memory	R1		mAP		
	@0.5	@0.7	@0.5	@0.75	Avg.
plain	63.74	49.68	64.10	47.74	46.21
sensitive	63.81	49.87	65.08	46.62	46.34
merged	65.10	51.61	65.41	48.56	47.61

(b) Choice of memory for boundary-focused attention

K	R1		mAP		
	@0.5	@0.7	@0.5	@0.75	Avg.
1 (fixed)	63.23	48.32	63.53	46.42	45.17
1	64.32	49.87	65.01	48.72	47.14
3	65.10	51.61	65.41	48.56	47.61
5	64.90	50.45	65.38	47.58	46.70

(c) Number of sampled boundary points

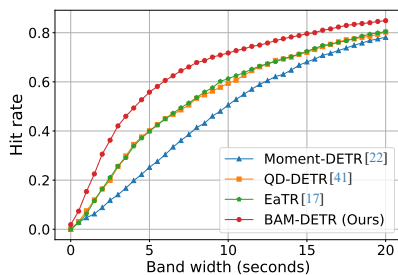
C_p	C_s	C_e	R1		mAP		
			@0.5	@0.7	@0.5	@0.75	Avg.
✓			62.97	49.03	64.44	47.50	46.26
	✓		64.39	50.71	64.60	47.69	46.66
		✓	64.58	49.23	64.38	47.85	46.71
✓	✓	✓	65.10	51.61	65.41	48.56	47.61

(d) Choice of queries for quality prediction

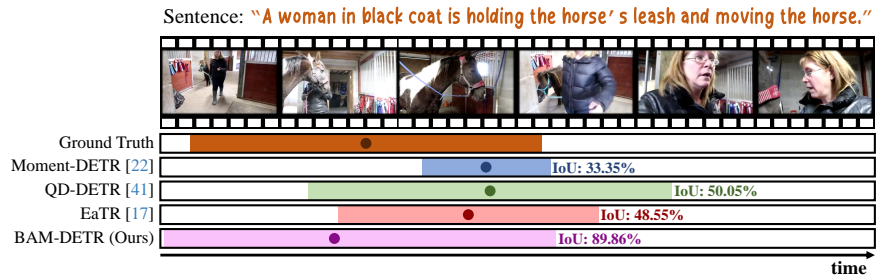
Anchor query	Boundary query	R1		mAP			FLOPs	Params
		@0.5	@0.7	@0.5	@0.75	Avg.		
Global (shared)		62.26	49.03	62.63	45.90	44.18	0.71G	8.2M
Global	Global	63.61	49.81	64.11	45.38	44.54	0.72G	11.5M
Global	Focused	63.74	49.68	64.10	47.74	46.21	0.65G	9.5M
Focused	Focused	62.48	49.16	63.90	47.31	45.87	0.62G	7.6M

(e) Combinations of attention layers for anchor and boundary updating pathways

Table 7. Ablative experiments on QVHighlights. Default settings are marked gray.



(a) Boundary hit rate with varying band widths.



(b) Visualization of the ground-truth moment and predictions by competitors.

Figure 4. Analytical experiments on QVHighlights.

Queries for quality prediction. We leverage both anchor and boundary queries for quality prediction. We investigate the effect of query choices in Table 7d. As a result, utilizing all the queries shows better localization performance than using one of them. This might be trivial as different queries contain complementary information for quality prediction.

Attention layers. Table 7e compares different combinations of attention layers in terms of performances and costs. For an apple-to-apple comparison, we leverage the plain memory features for both attention layers. First of all, employing separate global cross-attention for different queries leads to a huge parameter increase yet limited score gains. Replacing the global one for boundary queries with our focused attention layer substantially reduces the cost, while achieving the best performance. Meanwhile, the use of focused attention for both queries leads to inferior results.

Boundary alignment. Standard IoU-based metrics are indirect measures for boundary alignment. To precisely diagnose the ability, inspired by Deeplab [6], we compute the boundary hit rate of predictions with varying band widths. We expand ground-truth boundary points with a band width to form starting/ending zones and regard a prediction as correct if both of its boundaries fall within the corresponding zones. More details are in Appendix. To disentangle the effect of ranking, we mark a video as correct if at least one

prediction is correct and measure the video-level hit rate. As shown in Fig. 4a, our model greatly outperforms the recent competitors. The sharp increase in low band widths validates the superiority of our model in boundary alignment.

Qualitative results. As shown in Fig. 4b, previous models fail to localize accurate moments with misleading center predictions. In contrast, our model directly predicts well-aligned boundaries. More visualizations are in Appendix.

5. Conclusion

In this paper, we identified the center misalignment issue of existing query-based models for sentence grounding. To address it, we presented boundary-oriented moment modeling where boundaries are directly predicted without relying on centers. Based on the modeling, we designed the boundary-aligned moment detection transformer characterized by dual-pathway decoding. Further, we proposed localization quality-based scoring of predictions. The efficacy of the proposed methods is validated by thorough examinations. We hope this work sheds light on the issue of current center-based moment modeling in detection transformers.

Acknowledgements. This project was supported by the National Research Foundation of Korea grant funded by the Korea government (MSIT) (No. 2022R1A2B5B02001467).

References

- [1] Lisa Anne Hendricks, Oliver Wang, Eli Shechtman, Josef Sivic, Trevor Darrell, and Bryan Russell. Localizing moments in video with natural language. In *ICCV*, pages 5803–5812, 2017. [1](#), [6](#)
- [2] Meng Cao, Long Chen, Mike Zheng Shou, Can Zhang, and Yuexian Zou. On pursuit of designing multi-modal transformer for video grounding. In *EMNLP*, pages 9810–9823, 2021. [2](#)
- [3] Nicolas Carion, Francisco Massa, Gabriel Synnaeve, Nicolas Usunier, Alexander Kirillov, and Sergey Zagoruyko. End-to-end object detection with transformers. In *ECCV*, pages 213–229. Springer, 2020. [1](#), [3](#), [4](#), [5](#)
- [4] Jingyuan Chen, Xinpeng Chen, Lin Ma, Zequn Jie, and Tat-Seng Chua. Temporally grounding natural sentence in video. In *EMNLP*, pages 162–171, 2018. [2](#)
- [5] Long Chen, Chujie Lu, Siliang Tang, Jun Xiao, Dong Zhang, Chile Tan, and Xiaolin Li. Rethinking the bottom-up framework for query-based video localization. In *AAAI*, pages 10551–10558, 2020. [2](#)
- [6] Liang-Chieh Chen, George Papandreou, Iasonas Kokkinos, Kevin Murphy, and Alan L Yuille. Deeplab: Semantic image segmentation with deep convolutional nets, atrous convolution, and fully connected crfs. *PAMI*, 40(4):834–848, 2017. [8](#), [12](#)
- [7] Xiyang Dai, Yinpeng Chen, Jianwei Yang, Pengchuan Zhang, Lu Yuan, and Lei Zhang. Dynamic detr: End-to-end object detection with dynamic attention. In *ICCV*, pages 2988–2997, 2021. [3](#)
- [8] Alexey Dosovitskiy, Lucas Beyer, Alexander Kolesnikov, Dirk Weissenborn, Xiaohua Zhai, Thomas Unterthiner, Mostafa Dehghani, Matthias Minderer, Georg Heigold, Sylvain Gelly, et al. An image is worth 16x16 words: Transformers for image recognition at scale. In *ICLR*, 2021. [5](#)
- [9] Victor Escorcia, Mattia Soldan, Josef Sivic, Bernard Ghanem, and Bryan Russell. Temporal localization of moments in video collections with natural language. *arXiv preprint arXiv:1907.12763*, 2019. [1](#), [6](#)
- [10] Christoph Feichtenhofer, Haoqi Fan, Jitendra Malik, and Kaifeng He. Slowfast networks for video recognition. In *ICCV*, pages 6202–6211, 2019. [6](#)
- [11] Jiyang Gao, Chen Sun, Zhenheng Yang, and Ram Nevatia. Tall: Temporal activity localization via language query. In *CVPR*, pages 5267–5275, 2017. [1](#), [2](#), [6](#)
- [12] Peng Gao, Minghang Zheng, Xiaogang Wang, Jifeng Dai, and Hongsheng Li. Fast convergence of detr with spatially modulated co-attention. In *ICCV*, pages 3621–3630, 2021. [3](#)
- [13] Runzhou Ge, Jiyang Gao, Kan Chen, and Ram Nevatia. Mac: Mining activity concepts for language-based temporal localization. In *WACV*, pages 245–253. IEEE, 2019. [2](#)
- [14] Jort F Gemmeke, Daniel PW Ellis, Dylan Freedman, Aren Jansen, Wade Lawrence, R Channing Moore, Manoj Plakal, and Marvin Ritter. Audio set: An ontology and human-labeled dataset for audio events. In *ICASSP*, pages 776–780. IEEE, 2017. [6](#)
- [15] Soham Ghosh, Anuva Agarwal, Zarana Parekh, and Alexander G Hauptmann. Excl: Extractive clip localization using natural language descriptions. In *NAACL*, pages 1984–1990, 2019. [2](#)
- [16] Jiachang Hao, Haifeng Sun, Pengfei Ren, Jingyu Wang, Qi Qi, and Jianxin Liao. Can shuffling video benefit temporal bias problem: A novel training framework for temporal grounding. In *ECCV*, pages 130–147. Springer, 2022. [7](#)
- [17] Jinhyun Jang, Jungin Park, Jin Kim, Hyeongjun Kwon, and Kwanghoon Sohn. Knowing where to focus: Event-aware transformer for video grounding. In *ICCV*, pages 13846–13856, 2023. [1](#), [2](#), [4](#), [6](#), [13](#)
- [18] Qiuqiang Kong, Yin Cao, Turab Iqbal, Yuxuan Wang, Wenwu Wang, and Mark D Plumbley. Panns: Large-scale pretrained audio neural networks for audio pattern recognition. *IEEE/ACM Trans. on Audio, Speech, and Language Processing*, 28:2880–2894, 2020. [6](#)
- [19] Harold W Kuhn. The hungarian method for the assignment problem. *Naval research logistics quarterly*, 2(1-2):83–97, 1955. [5](#)
- [20] Pilhyeon Lee, Taeh Kim, Minh Shim, Dongyoon Wee, and Hyeran Byun. Decomposed cross-modal distillation for rgb-based temporal action detection. In *CVPR*, pages 2373–2383, 2023. [1](#)
- [21] Jie Lei, Licheng Yu, Tamara L Berg, and Mohit Bansal. Tvr: A large-scale dataset for video-subtitle moment retrieval. In *ECCV*, pages 447–463. Springer, 2020. [6](#)
- [22] Jie Lei, Tamara L Berg, and Mohit Bansal. Detecting moments and highlights in videos via natural language queries. In *Neurips*, pages 11846–11858, 2021. [1](#), [2](#), [3](#), [4](#), [5](#), [6](#), [7](#), [12](#), [13](#)
- [23] Feng Li, Hao Zhang, Shilong Liu, Jian Guo, Lionel M Ni, and Lei Zhang. Dn-detr: Accelerate detr training by introducing query denoising. In *CVPR*, pages 13619–13627, 2022. [3](#)
- [24] Feng Li, Ailing Zeng, Shilong Liu, Hao Zhang, Hongyang Li, Lei Zhang, and Lionel M Ni. Lite detr: An interleaved multi-scale encoder for efficient detr. In *CVPR*, pages 18558–18567, 2023. [3](#)
- [25] Hongxiang Li, Meng Cao, Xuxin Cheng, Yaowei Li, Zhihong Zhu, and Yuexian Zou. G2l: Semantically aligned and uniform video grounding via geodesic and game theory. In *ICCV*, pages 12032–12042, 2023. [2](#)
- [26] Pandeng Li, Chen-Wei Xie, Hongtao Xie, Liming Zhao, Lei Zhang, Yun Zheng, Deli Zhao, and Yongdong Zhang. Momentdiff: Generative video moment retrieval from random to real. In *Neurips*, 2023. [1](#), [2](#), [4](#), [6](#), [7](#)
- [27] Chuming Lin, Chengming Xu, Donghao Luo, Yabiao Wang, Ying Tai, Chengjie Wang, Jilin Li, Feiyue Huang, and Yanwei Fu. Learning salient boundary feature for anchor-free temporal action localization. In *CVPR*, pages 3320–3329, 2021. [5](#)
- [28] Kevin Qinghong Lin, Pengchuan Zhang, Joya Chen, Shraman Pramanick, Difei Gao, Alex Jinpeng Wang, Rui Yan, and Mike Zheng Shou. Univtg: Towards unified video-language temporal grounding. In *ICCV*, pages 2794–2804, 2023. [2](#), [3](#), [4](#), [6](#), [7](#)
- [29] Tianwei Lin, Xu Zhao, Haisheng Su, Chongjing Wang, and Ming Yang. Bsn: Boundary sensitive network for temporal

- action proposal generation. In *ECCV*, pages 3–19, 2018. [1](#), [5](#)
- [30] Yutong Lin, Yuhui Yuan, Zheng Zhang, Chen Li, Nanning Zheng, and Han Hu. Detr does not need multi-scale or locality design. In *ICCV*, pages 6545–6554, 2023. [3](#)
- [31] Daizong Liu, Xiaoye Qu, Jianfeng Dong, Pan Zhou, Yu Cheng, Wei Wei, Zichuan Xu, and Yulai Xie. Context-aware biaffine localizing network for temporal sentence grounding. In *CVPR*, pages 11235–11244, 2021. [2](#)
- [32] Daizong Liu, Xiaoye Qu, Jianfeng Dong, Pan Zhou, Yu Cheng, Wei Wei, Zichuan Xu, and Yulai Xie. Context-aware biaffine localizing network for temporal sentence grounding. In *CVPR*, pages 11235–11244, 2021. [1](#)
- [33] Fanfan Liu, Haoran Wei, Wenzhe Zhao, Guozhen Li, Jingquan Peng, and Zihao Li. Wb-detr: transformer-based detector without backbone. In *ICCV*, pages 2979–2987, 2021. [3](#)
- [34] Meng Liu, Xiang Wang, Liqiang Nie, Qi Tian, Baoquan Chen, and Tat-Seng Chua. Cross-modal moment localization in videos. In *ACM MM*, pages 843–851, 2018. [2](#)
- [35] Shilong Liu, Feng Li, Hao Zhang, Xiao Yang, Xianbiao Qi, Hang Su, Jun Zhu, and Lei Zhang. Dab-detr: Dynamic anchor boxes are better queries for detr. In *ICLR*, 2022. [3](#), [4](#)
- [36] Shilong Liu, Tianhe Ren, Jiayu Chen, Zhaoyang Zeng, Hao Zhang, Feng Li, Hongyang Li, Jun Huang, Hang Su, Jun Zhu, and Lei Zhang. Detection transformer with stable matching. In *ICCV*, pages 6491–6500, 2023. [3](#)
- [37] Ye Liu, Siyuan Li, Yang Wu, Chang-Wen Chen, Ying Shan, and Xiaohu Qie. Umt: Unified multi-modal transformers for joint video moment retrieval and highlight detection. In *CVPR*, pages 3042–3051, 2022. [1](#), [2](#), [3](#), [6](#)
- [38] Ilya Loshchilov and Frank Hutter. Decoupled weight decay regularization. In *ICLR*, 2019. [6](#)
- [39] Chujie Lu, Long Chen, Chilie Tan, Xiaolin Li, and Jun Xiao. Debug: A dense bottom-up grounding approach for natural language video localization. In *EMNLP-IJCNLP*, pages 5144–5153, 2019. [2](#)
- [40] Depu Meng, Xiaokang Chen, Zejia Fan, Gang Zeng, Houqiang Li, Yuhui Yuan, Lei Sun, and Jingdong Wang. Conditional detr for fast training convergence. In *ICCV*, pages 3651–3660, 2021. [3](#), [4](#)
- [41] WonJun Moon, Sangeek Hyun, SangUk Park, Dongchan Park, and Jae-Pil Heo. Query-dependent video representation for moment retrieval and highlight detection. In *CVPR*, pages 23023–23033, 2023. [1](#), [2](#), [3](#), [4](#), [6](#), [7](#), [12](#), [13](#)
- [42] Jonghwan Mun, Minsu Cho, and Bohyung Han. Local-global video-text interactions for temporal grounding. In *CVPR*, pages 10810–10819, 2020. [2](#), [3](#)
- [43] Jeffrey Pennington, Richard Socher, and Christopher D Manning. Glove: Global vectors for word representation. In *EMNLP*, pages 1532–1543, 2014. [7](#)
- [44] Alec Radford, Jong Wook Kim, Chris Hallacy, Aditya Ramesh, Gabriel Goh, Sandhini Agarwal, Girish Sastry, Amanda Askell, Pamela Mishkin, Jack Clark, et al. Learning transferable visual models from natural language supervision. In *ICML*, pages 8748–8763. PMLR, 2021. [6](#)
- [45] Michaela Regneri, Marcus Rohrbach, Dominikus Wetzel, Stefan Thater, Bernt Schiele, and Manfred Pinkal. Grounding action descriptions in videos. *Trans. Assoc. Comput. Linguistics*, 1:25–36, 2013. [6](#)
- [46] Hamid Rezaatofghi, Nathan Tsoi, JunYoung Gwak, Amir Sadeghian, Ian Reid, and Silvio Savarese. Generalized intersection over union: A metric and a loss for bounding box regression. In *CVPR*, pages 658–666, 2019. [5](#)
- [47] Byungseok Roh, JaeWoong Shin, Wuhyun Shin, and Sae-hoon Kim. Sparse detr: Efficient end-to-end object detection with learnable sparsity. In *ICLR*, 2022. [3](#)
- [48] Yong Rui, Anoop Gupta, and Alex Acero. Automatically extracting highlights for tv baseball programs. In *ACM MM*, pages 105–115, 2000. [1](#)
- [49] Dian Shao, Yu Xiong, Yue Zhao, Qingqiu Huang, Yu Qiao, and Dahua Lin. Find and focus: Retrieve and localize video events with natural language queries. In *ECCV*, pages 200–216, 2018. [1](#)
- [50] Aidean Sharghi, Jacob S Laurel, and Boqing Gong. Query-focused video summarization: Dataset, evaluation, and a memory network based approach. In *CVPR*, pages 4788–4797, 2017. [1](#)
- [51] Dingfeng Shi, Yujie Zhong, Qiong Cao, Lin Ma, Jia Li, and Dacheng Tao. Tridet: Temporal action detection with relative boundary modeling. In *CVPR*, pages 18857–18866, 2023. [5](#)
- [52] Karen Simonyan and Andrew Zisserman. Very deep convolutional networks for large-scale image recognition. In *ICLR*, 2015. [7](#)
- [53] Zhiqing Sun, Shengcao Cao, Yiming Yang, and Kris M Kitani. Rethinking transformer-based set prediction for object detection. In *ICCV*, pages 3611–3620, 2021. [3](#)
- [54] Ashish Vaswani, Noam Shazeer, Niki Parmar, Jakob Uszkoreit, Llion Jones, Aidan N Gomez, Łukasz Kaiser, and Illia Polosukhin. Attention is all you need. In *Neurips*, 2017. [3](#), [4](#)
- [55] Yingming Wang, Xiangyu Zhang, Tong Yang, and Jian Sun. Anchor detr: Query design for transformer-based detector. In *AAAI*, pages 2567–2575, 2022. [3](#)
- [56] Zhenzhi Wang, Limin Wang, Tao Wu, Tianhao Li, and Gangshan Wu. Negative sample matters: A renaissance of metric learning for temporal grounding. In *AAAI*, pages 2613–2623, 2022. [2](#), [7](#)
- [57] Shaoning Xiao, Long Chen, Songyang Zhang, Wei Ji, Jian Shao, Lu Ye, and Jun Xiao. Boundary proposal network for two-stage natural language video localization. In *AAAI*, pages 2986–2994, 2021. [2](#)
- [58] Bo Xiong, Yannis Kalantidis, Deepti Ghadiyaram, and Kristen Grauman. Less is more: Learning highlight detection from video duration. In *CVPR*, pages 1258–1267, 2019. [1](#)
- [59] Huijuan Xu, Kun He, Bryan A Plummer, Leonid Sigal, Stan Sclaroff, and Kate Saenko. Multilevel language and vision integration for text-to-clip retrieval. In *AAAI*, pages 9062–9069, 2019. [2](#)
- [60] Yifang Xu, Yunzhuo Sun, Yang Li, Yilei Shi, Xiaoxiang Zhu, and Sidan Du. Mh-detr: Video moment and highlight detection with cross-modal transformer. In *ACM MM*, 2023. [2](#), [6](#)

- [61] Shen Yan, Xuehan Xiong, Arsha Nagrani, Anurag Arnab, Zhonghao Wang, Weina Ge, David Ross, and Cordelia Schmid. Unloc: A unified framework for video localization tasks. In *ICCV*, pages 13623–13633, 2023. [2](#)
- [62] Mingqiao Ye, Lei Ke, Siyuan Li, Yu-Wing Tai, Chi-Keung Tang, Martin Danelljan, and Fisher Yu. Cascade-detr: Delving into high-quality universal object detection. In *ICCV*, pages 6704–6714, 2023. [3](#)
- [63] Yitian Yuan, Lin Ma, Jingwen Wang, Wei Liu, and Wenwu Zhu. Semantic conditioned dynamic modulation for temporal sentence grounding in videos. In *Neurips*, 2019. [1](#), [2](#)
- [64] Yitian Yuan, Tao Mei, and Wenwu Zhu. To find where you talk: Temporal sentence localization in video with attention based location regression. In *AAAI*, pages 9159–9166, 2019. [2](#)
- [65] Yitian Yuan, Xiaohan Lan, Xin Wang, Long Chen, Zhi Wang, and Wenwu Zhu. A closer look at temporal sentence grounding in videos: Dataset and metric. In *Proc. 2nd Int. Workshop on Human-Centric Multimedia Analysis*, pages 13–21, 2021. [7](#)
- [66] Runhao Zeng, Haoming Xu, Wenbing Huang, Peihao Chen, Mingkui Tan, and Chuang Gan. Dense regression network for video grounding. In *CVPR*, pages 10287–10296, 2020. [2](#)
- [67] Da Zhang, Xiyang Dai, Xin Wang, Yuan-Fang Wang, and Larry S Davis. Man: Moment alignment network for natural language moment retrieval via iterative graph adjustment. In *CVPR*, pages 1247–1257, 2019. [2](#)
- [68] Gongjie Zhang, Zhipeng Luo, Yingchen Yu, Kaiwen Cui, and Shijian Lu. Accelerating detr convergence via semantic-aligned matching. In *CVPR*, pages 949–958, 2022. [3](#)
- [69] Hao Zhang, Aixin Sun, Wei Jing, and Joey Tianyi Zhou. Span-based localizing network for natural language video localization. In *ACL*, 2020. [2](#), [3](#), [7](#)
- [70] Hao Zhang, Feng Li, Shilong Liu, Lei Zhang, Hang Su, Jun Zhu, Lionel Ni, and Heung-Yeung Shum. Dino: Detr with improved denoising anchor boxes for end-to-end object detection. In *ICLR*, 2023. [3](#)
- [71] Ke Zhang, Wei-Lun Chao, Fei Sha, and Kristen Grauman. Video summarization with long short-term memory. In *ECCV*, pages 766–782. Springer, 2016. [1](#)
- [72] Songyang Zhang, Jinsong Su, and Jiebo Luo. Exploiting temporal relationships in video moment localization with natural language. In *ACM MM*, pages 1230–1238, 2019. [2](#)
- [73] Songyang Zhang, Houwen Peng, Jianlong Fu, and Jiebo Luo. Learning 2d temporal adjacent networks for moment localization with natural language. In *AAAI*, pages 12870–12877, 2020. [1](#), [2](#), [3](#), [7](#)
- [74] Zhu Zhang, Zhijie Lin, Zhou Zhao, and Zhenxin Xiao. Cross-modal interaction networks for query-based moment retrieval in videos. In *ACM SIGIR*, pages 655–664, 2019. [2](#)
- [75] Yue Zhao, Yuanjun Xiong, Limin Wang, Zhirong Wu, Xiaoou Tang, and Dahua Lin. Temporal action detection with structured segment networks. In *ICCV*, pages 2914–2923, 2017. [1](#)
- [76] Dehua Zheng, Wenhui Dong, Hailin Hu, Xinghao Chen, and Yunhe Wang. Less is more: Focus attention for efficient detr. In *ICCV*, pages 6674–6683, 2023. [3](#)
- [77] Xizhou Zhu, Han Hu, Stephen Lin, and Jifeng Dai. Deformable convnets v2: More deformable, better results. In *CVPR*, pages 9308–9316, 2019. [5](#)
- [78] Xizhou Zhu, Weijie Su, Lewei Lu, Bin Li, Xiaogang Wang, and Jifeng Dai. Deformable detr: Deformable transformers for end-to-end object detection. In *ICLR*, 2021. [3](#), [4](#), [5](#), [12](#)

This appendix provides the following content.

- Formulation of saliency losses (Sec. A)
- Comparison with Deformable DETR (Sec. B)
- Details of boundary alignment evaluation (Sec. C)
- More analyses of the proposed methods (Sec. D)
- Further qualitative results (Sec. E)

A. Formulation of Saliency Losses

As mentioned in the main paper, we adopt saliency losses for effective multimodal alignment in the encoder, following the convention [22, 41]. In specific, our total saliency-based loss is composed of three losses, *i.e.*, $\mathcal{L}_{\text{sal}} = \mathcal{L}_{\text{margin}} + \mathcal{L}_{\text{cont}} + \mathcal{L}_{\text{neg}}$. The margin-based loss $\mathcal{L}_{\text{margin}}$, as defined in Eq. (2) of the main paper, aims to encourage the model to produce higher saliency scores for the clips relevant to the given sentence compared to less related clips. Meanwhile, the rank-aware contrastive loss $\mathcal{L}_{\text{cont}}$ is utilized to preserve the ground-truth clip ranking in prediction scores. To be concrete, we define the positive and negative sets based on a reference score r : clips with saliency score labels higher than r form the positive set \mathcal{B}_r^+ , and the remaining clips constitute the negative set \mathcal{B}_r^- . The rank-aware contrastive loss is then formulated with a set of reference scores \mathcal{R} as:

$$\mathcal{L}_{\text{cont}} = - \sum_{v_r \in \mathcal{R}} \log \frac{\sum_{\forall \hat{v} \in \mathcal{B}_r^+} \exp(S(\hat{v})/\tau)}{\sum_{\forall \hat{v} \in (\mathcal{B}_r^+ \cup \mathcal{B}_r^-)} \exp(S(\hat{v})/\tau)}, \quad (10)$$

where $S(\cdot)$ is a saliency score predictor and τ is a temperature (set to 0.5). We define \mathcal{R} to be the set of saliency score labels of positive clips within ground-truth moments.

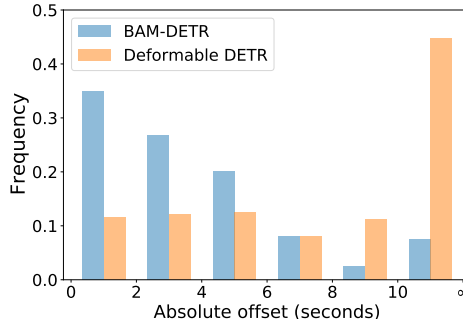
The negative relation loss is based on the assumption that all video clips should exhibit low saliency scores when paired with unmatched (negative) sentences. Formally, the loss is defined as follows.

$$\mathcal{L}_{\text{neg}} = - \sum_{\forall \hat{v}^{\text{neg}} \in \hat{\mathcal{V}}^{\text{neg}}} \log(1 - S(\hat{v}^{\text{neg}})), \quad (11)$$

where $\hat{\mathcal{V}}^{\text{neg}}$ denotes the memory features obtained by processing the video with a negative sentence through the encoder. In our implementation, a negative sentence is sampled from a different video-sentence pair in the mini-batch.

B. Comparison with Deformable DETR

Our boundary-focused attention layer incorporates deformable attention, which is first proposed in Deformable DETR [78]. It was originally designed for computationally efficient global attention with multi-scale features in object detection. In contrast, we employ deformable attention for local aggregation of neighbor features, aiding precise boundary prediction in temporal sentence grounding. To elucidate the discrepancy in their roles, we conduct a comparative experiment. For this study, we implement a 1D



of l_w to form boundary zones. We can denote the starting and ending zones by $Z_{s_n} = [t_{s_n} - 0.5l_w, t_{s_n} + 0.5l_w]$ and $Z_{e_n} = [t_{e_n} - 0.5l_w, t_{e_n} + 0.5l_w]$, respectively. Then, for the m -th proposal $\{\hat{t}_{s_m}, \hat{t}_{e_m}\}$, we check whether both of its boundaries fall in the corresponding zones. We iterate this process for all combinations of ground truths and predictions, and mark a video as correct if any pair is positive. Formally, the binary variable of h of a video is defined as:

$$h = \max_{\forall n, m} [\text{Hit}^s(n, m) \cdot \text{Hit}^e(n, m)],$$

where $\text{Hit}^z(n, m) = \mathbb{1}[|\hat{t}_{z_m} - t_{z_n}| \leq 0.5l_w]$, $z \in \{s, e\}$.

We measure the hit rate over the whole validation set.

D. More Analyses

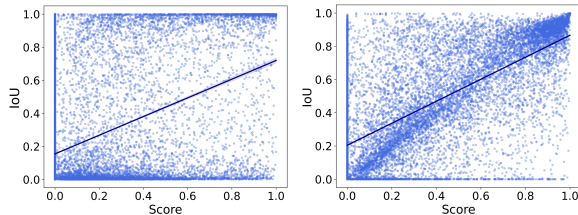
Ablation on loss functions. Our model employs several loss functions for training. We conduct an ablative experiment to diagnose their effects. Table A2 summarizes the results, where the upper part adopts the typical classification-based scoring whereas the lower one leverages our proposed quality-based scoring. We first examine the benefit of saliency losses. Consistent with the recent findings [22], we observe notable performance gains brought by the better cross-modal alignment in the encoder. Then we investigate the importance of our regularization loss (*cf.*, Eq. (5) of the main paper) designed for boundary-sensitive feature construction. It can be observed that regardless of the choice of scoring methods, the boundary regularization leads to significant performance boosts. Putting together the results in Table 7b of the main paper, it becomes clear that boundary-sensitive features are essential for precise boundary updating. Lastly, the comparison between the two separate parts validates the efficacy of our quality-based scoring.

Comparison between scoring methods. We present the quality-based scoring method to replace the conventional classification-based one. To compare two scoring methods, we draw scatter plots of scores *vs.* IoUs with ground truths using all predictions on the QVHighlights validation set. Fig. A2a indicates that classification scores correlate with IoUs to an extent. Meanwhile, we observe in Fig. A2b that our quality-based scoring shows a much stronger correlation, leading to better proposal ranking. These results validate its efficacy in estimating the localization qualities of proposals, rather than the matching degree.

Generalizability of the quality-based scoring. By design, our quality-based scoring is generalizable to any query-based approach. To investigate this property, we conduct experiments with three representative models: Moment-DETR [22], QD-DETR [41], and EaTR [17]. The results are shown in Table A3, where the proposed scoring method brings consistent improvements over different baselines. Noticeably, we observe the pronounced gains at high

\mathcal{L}_{loc}	\mathcal{L}_{cls}	$\mathcal{L}_{\text{qual}}$	\mathcal{L}_{sal}	$\mathcal{L}_{\text{regul}}$	R1		mAP		
					@0.5	@0.7	@0.5	@0.75	Avg.
✓	✓				56.77	41.03	58.63	39.25	39.12
✓	✓		✓		60.58	46.65	62.09	43.83	42.94
✓	✓		✓	✓	63.61	50.26	63.01	44.98	44.16
✓		✓			59.23	46.13	60.52	44.80	43.48
✓		✓	✓		63.23	50.00	64.03	47.42	46.64
✓		✓	✓	✓	65.10	51.61	65.41	48.56	47.61

Table A2. Ablation study on the loss functions on QVHighlights.



(a) Classification-based scoring (b) Quality-based scoring

Figure A2. Correlation between scores and IoUs with ground truths: (a) the classification scores show a moderate correlation (Pearson’s r of 0.44); (b) the quality scores exhibit a stronger correlation (Pearson’s r of 0.67).

Method	R1		mAP		
	@0.5	@0.7	@0.5	@0.75	Avg.
Moment-DETR [‡] [22]	53.23	34.00	54.80	29.02	30.58
+ quality-based scoring	56.77	38.65	55.09	35.30	34.98
QD-DETR [‡] [41]	62.90	46.77	62.66	41.51	41.24
+ quality-based scoring	64.26	50.32	63.79	46.03	44.50
EaTR [‡] [17]	57.74	42.71	59.40	39.34	39.06
+ quality-based scoring	59.42	45.61	60.24	42.29	41.61

[‡]All models are reproduced by official codebase

Table A3. Generalizability evaluation of quality-based scoring on the QVHighlights validation split.

IoU thresholds, indicating better fitting of proposals with the ground truths. This corroborates our claim that moment proposals ought to be ranked based on their localization qualities rather than the degree of matching.

E. Further Qualitative Results

We perform further qualitative comparisons with previous query-based methods in Fig. A3 and Fig. A4. The comparison results across various scenarios demonstrate the superiority of our BAM-DETR over strong competitors.

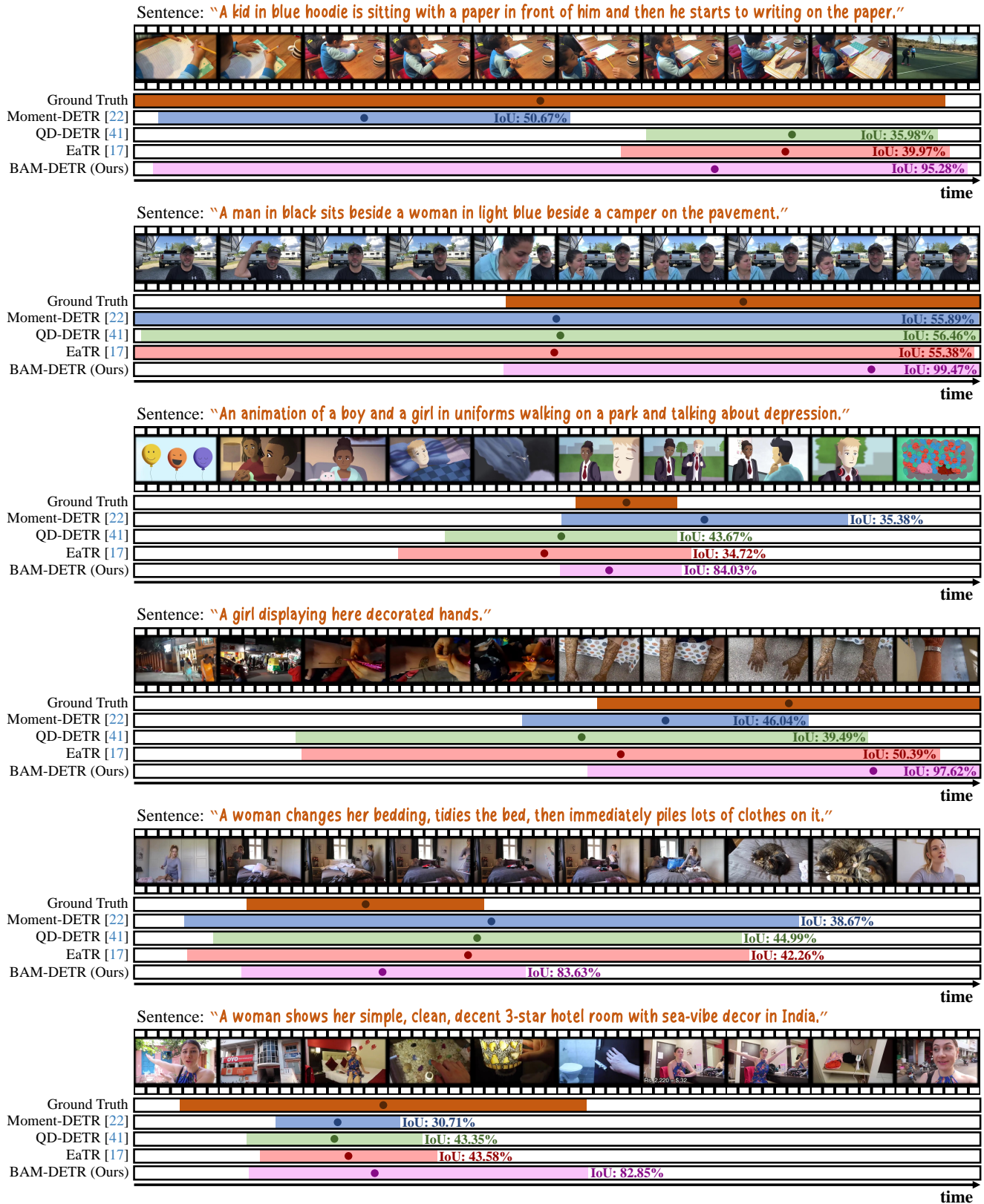


Figure A3. Qualitative comparison on the QVHighlights validation split.



Figure A4. Qualitative comparison on the QVHighlights validation split.